Compositions, structures, and properties of nickel-containing minerals in the kerolite–pimelite series

G. W. Brindley, David L. Bish[1] and Hsien-Ming Wan[2]

Mineral Sciences Building, The Pennsylvania State University
University Park, Pennsylvania 16802

Abstract

The term kerolite–pimelite series is used for a series of hydrous magnesium–nickel silicates with talc-like structure and composition but with additional water and with a highly disordered and non-swelling stacking of the layers. The layer spacing, obtained after correction for Lorentz-polarization and structure factor variations with diffraction angle, is near 9.6A and is larger than that of talc because of an absence of close-packing of adjacent layers. The average composition of nineteen samples is $(Mg,Ni)_{3.04}(Al,Fe)_{0.01}(Si_{3.93}Al_{0.02}Fe_{0.02})O_{10}$ $(OH)_2 \cdot 0.89H_2O$. The additional "water" is held in a variety of ways and is released gradually up to 700°C. Infrared spectroscopic data suggest the presence of surface hydroxyls yielding an absorption near 3700 cm^{-1}, Si–OH groups with absorption near 4550 cm^{-1}, and interlayer and surface adsorbed H_2O absorbing at 1600, 3400, and 3600 cm^{-1}. The splitting of OH stretching and librational modes in the infrared spectra clearly shows the effects of increasing Ni-for-Mg substitution. As expected, optical absorption spectra provide evidence for Ni^{2+} in octahedral coordination only. The thermal transformations of these minerals are examined, and evidence is obtained for a transitional face-centered cubic phase prior to the development of a high-temperature phase.

Introduction

The term "kerolite–pimelite series" is used in the sense defined by Maksimovic (1966) and Brindley and Maksimovic (1974) for a series of magnesium–nickel hydrous silicates with essentially talc-like compositions and highly disordered, non-swelling stacking of the layers. The relation of the magnesium end-member, kerolite, to talc and stevensite has been discussed by Brindley *et al.* (1977). The present study extends this work to similar nickel-containing minerals which are named pimelites when the atomic proportion of Ni exceeds that of Mg.

A major problem in this study, as in the previous work on the lizardite–nepouite series (Brindley and Wan, 1975), was to obtain material sufficiently pure mineralogically to merit detailed examination. These nickel-containing minerals commonly occur as intimate mixtures and are called garnierites (Pecora *et al.*, 1949); they are analogous to the magnesium-containing deweylites (Bish and Brindley, 1978). Because it is virtually impossible to separate the components, the only available course is to examine large numbers of samples and to select those mainly of one or other type. In the study of garnierites by Brindley and Pham Thi Hang (1973), only six nickeloan kerolites and pimelites were available, and two of these contained appreciable serpentine impurity; in the present work eighteen samples have been obtained, so that we are now in a better position to study this series of minerals.

Experimental procedures

Preliminary selection of material was made under a binocular microscope by hand-picking green, clay-like materials (garnierites). X-ray examination then showed if the selected material belonged to the lizardite–nepouite series (basal spacing about 7.3A), or the kerolite-pimelite series (basal spacing about 10A), or a mixture of the two. In practice, the selection of monomineralic material is often less certain than this simple description suggests, because the only distinguishing features are the 001 and 002 reflections of

the 7.3A phase and the 001 and 003 reflections of the 10A phase. These reflections are commonly broad, and small proportions, such as 5 percent or even more, of one component in the presence of the other can easily be overlooked. All other diffraction features tend to be of the two-dimensional type because of layer stacking disorder, and they overlap completely for the two series. Nevertheless, with care and a practiced eye, mainly monomineralic samples can be selected.

Samples containing predominantly a 10A spacing mineral were separated from coarse impurities (particle size greater than about 10–20 μm) by ultrasonic dispersal in water and settling under gravity. The fine fraction, less than a few microns particle size, was allowed to dry at ~40°C in air. Further X-ray examination, usually of thin oriented samples on glass slides, was made to check for contamination by other layer silicates and for any changes of basal spacings with humidity (0–100 percent RH in controlled atmospheres), with ethylene glycol vapor (usually for several days at ~50°C), and after heat treatment (various temperatures up to 550°C).

Chemical analysis of suitable materials was made by atomic absorption methods using the lithium metaborate fusion technique of Medlin *et al.* (1969). The ignition loss of materials heated to 1100°C after previous drying at 110°C was determined, and the ignited material was used for the total analysis.

Combined gravimetric and X-ray diffraction data were obtained by taking two samples of each material studied, which were given identical heat treatments, mainly 3–4 hr heatings at a sequence of temperatures 50°–100°C apart. One sample was used solely for gravimetric measurements and the other for X-ray examination. By this procedure, weight (water) loss was correlated with structural changes.

Spectroscopic analyses were made in the near-infrared and visible regions using a diffuse reflectance attachment to a Beckman DK-2A spectrometer. Infrared spectra were obtained with the KBr pellet technique and a Perkin-Elmer spectrophotometer, model 621.

X-ray diffraction data

Table 1 records d spacings and 00l and hk indices for representative samples. Diffractometer patterns have been published previously by Maksimovic (1966) and by Brindley and Pham Thi Hang (1973). The apparent values of d(001), taken directly from diffraction recordings, are usually in the range 9.8–10.2A, but when corrected for the variation of the Lorentz-polarization factor and the structure factor over the range of 2θ values involved, the value of d(001) is near 9.6±0.05A and agrees with $3 \times d$(003) $\simeq$ 9.55A. The increase in the basal spacing as compared with the value for talc, about 9.35–9.38A, is attributed to the random stacking of the layers which does not permit their partial close-packing as in the structure of talc (see Rayner and Brown, 1973). The 002 diffraction peak is always weak and is resolved only partially from the adjacent 02, 11 diffraction band. It is seen more clearly from Mg-rich than from Ni-rich samples. Calculated intensity ratios, I(001):I(002):I(003) are respectively 100:7:41 and 100:3:15 for the Mg- and Ni-end-members; the calculations assume the z atomic parameters for talc given by Rayner and Brown (1973). The sharp 06 diffraction band corresponds closely to the 060 position and gives a value of b = 9.15A.

The effect of the Lp and structure factor variations on the apparent basal spacings, d'(001) and $2d'$(002), of talc crystallites containing small numbers of layers is shown by the following calculated values:

No. of layers	3	4	6	10	12	∞
d'(001), A	10.98	10.30	9.81	9.54	9.45	9.35
$2d'$(002), A	9.91	9.71	9.51	9.38	9.38	9.35

Evidently the number of layers must exceed about 20 before the effect becomes negligible.

The angular breadth B of the basal diffraction profiles at half-maximum intensity, after correction for instrumental broadening, gives the average thickness t of the crystallites by application of the Scherrer equation, Bcos θ = $0.9\lambda/t$, provided broadening arises only from small crystal size. On this basis, values of t of the order of 40–60A or 4–7 structural layers are obtained. The mean diameter D of the crystallites is estimated similarly from the profile of the 02, 11 diffraction band using the expression given by Warren and Bodenstein (1965): Bcos θ = $1.91\lambda/D$. Values obtained range from about 90–170A.

The question whether kerolites and pimelites are swelling or non-swelling minerals is crucial in deciding whether they belong to the smectite group or to the talc–willemseite group; willemseite is a nickel-rich form of talc described by DeWaal (1970). We have already shown that kerolites are essentially non-swelling minerals (Brindley *et al.*, 1977). Similar tests have been made for nickeloan kerolites and pimelites. Samples were exposed for several days or longer to various relative humidities, to ethylene glycol vapor, and to various low-temperature heat treatments. Representative results are shown in Figure 1. The

Table 1. X-ray powder diffraction data for representative kerolites and pimelites

hk and 00ℓ	1 (a) d	I	2 (b) d	I	3 (b) d	I	4 (a) d	I	5 (b) d	I
001	10.0	65	9.8	100	9.6	100	9.6	100	9.6	100
002	4.83	15	–	–	–	–	4.73	15	–	–
02,11	4.54	100	4.59	100	4.56	70	4.54	60	4.56	70
003	3.19	55	3.18	70	3.19	50	3.15	70	3.17	50
13,20	2.55	50	2.62	75	2.62	70	2.53	55	2.62	60
04,22	2.28	25	2.31	30	–	–	–	–	2.27	15
15,24,31	1.72	15	1.725	20	1.73	20	1.72	10	1.73	30
06,33	1.522	50	1.525	100	1.528	100	1.524	45	1.526	100
26,40	1.314	20	1.317	20	1.316	30	1.315	10	1.317	30
17,35,42	1.268	5	1.265	20	1.274	5	–	–	1.267	10

1. Kerolite from Carter's Mine, N. Carolina. Dried at 110°C
2. Nickeloan kerolite, sample (6) of Table 2; room conditions
3. Nickeloan kerolite, sample (8) of Table 2; room conditions
4. Nickeloan kerolite, sample (8) of Table 2; after 650°C heating
5. Pimelite, sample (17) of Table 2; room conditions
   (a) Diffractometer data; (b) Debye-Scherrer camera data

compositions of the samples, listed in Table 2, are discussed later. The various treatments used are listed in the caption to Figure 1. From patterns labelled (b), samples in 100 percent RH, to patterns labelled (f), samples after 550°C for 3 hr, no change in peak position is observed, but some samples do show a sharpening of the peak profile. This result suggests that the layer spacings become somewhat more regular with the heat treatment, but there is no obvious improvement in the layer stacking order. The results indicate an absence of swelling in humid atmospheres and show that these minerals are not smectites.

Their behavior with respect to ethylene glycol vapor is less simple but still confirms that they are distinctly different from smectites which expand readily in ethylene glycol to give a regularly expanded spacing of about 17A. When exposed for long periods, the basal spacings of kerolites and pimelites in some cases show modifications which suggest a partial penetration of glycol into the structures. Samples (1), (13) and (18) [see Figs. 1(a), (c), (e)] show these effects; samples (10) and (17) [see Figs. 1(b), (d)] do not show these effects. Evidently when penetration occurs it is partial and irregular, as shown by the poorly defined diffraction effect. The mechanism by which ethylene glycol causes expansion of smectites is still poorly understood but probably is quite different from the expansion caused by water which is related to cation hydration. Ethylene glycol will penetrate into reduced charge montmorillonites when water will not penetrate (Brindley and Ertem, 1971). Possibly glycol penetrates because of an interaction with the Si–O surfaces of the layers. Since the layer stacking in kerolites and pimelites is extremely disordered, such that the layer spacing is near 9.6A as compared with 9.35A for talc, there may well be regions where the normal interlayer bonding is appreciably or even considerably reduced. The calculations of Giese (1975) show that the interlayer bonding in talc and pyrophyllite is partially ionic and is considerably reduced when the layer spacing is increased; an increase of spacing from 9.35 to 9.6A produces a 40 percent decrease in the ionic and van der Waals forces of interlayer attraction. Regions of weaker bonding could well be the cause of a partial penetration of ethylene glycol.
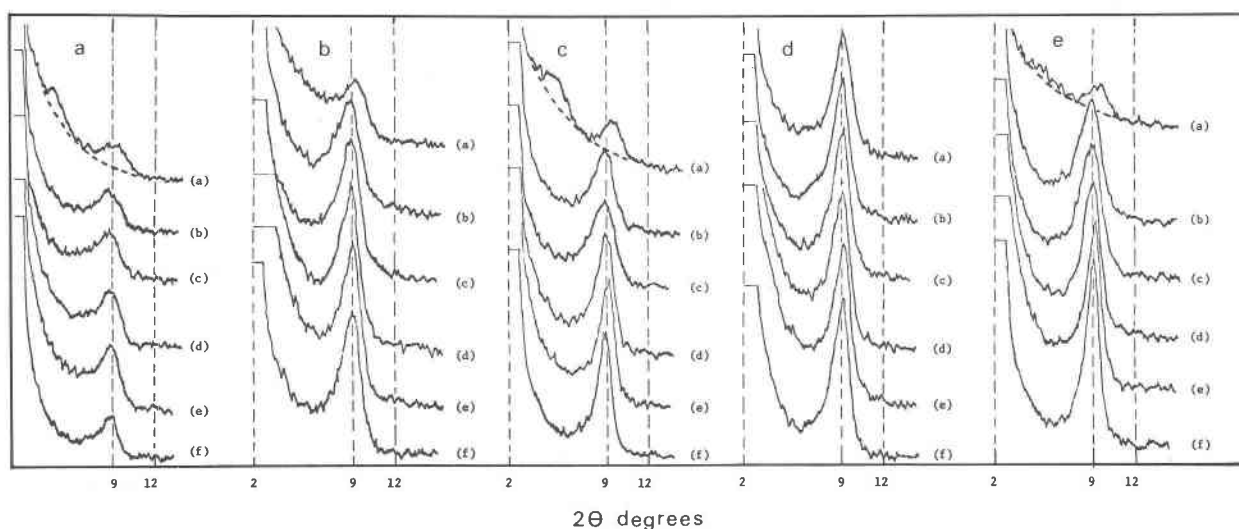

Fig. 1. Diffractometer patterns of 001 reflections from kerolites and pimelites; Ni-filtered, CuKα radiation. Figs. (a)–(e) correspond to samples (1), (10), (13), (17), (18) of Table 2. Treatments of samples are as follows: (a) exposed to ethylene glycol vapor, 25°C, 4 weeks; (b) and (c) exposed to 100 percent and 50 percent relative humidity; (d), (e), (f) heated at 110°C, 350°C, 555°C for 3 hr and cooled in desiccator.

Table 2. Chemical analyses and formulae of minerals in the kerolite–pimelite series

	(1)	(2)	(3)	(4)	(5)	(6)	(7)	(8)	(9)	(10)	(11)	(12)	(13)	(14)	(15)	(16)	(17)	(18)	(19)
SiO_2	58.63	54.6	57.3	55.2	54.4	55.7	54.1	55.5	55.4	53.3	54.9	51.4	53.5	53.5	51.1	52.3	52.0	50.6	48.1
TiO_2	-	-	0.08	-	-	-	-	-	0.01	0.01	-	-	0.10	0.00	0.02	0.07	0.07	0.08	0.08
Al_2O_3	0.05	0.29	0.03	0.38	0.31	0.24	0.10	0.31	0.16	0.18	0.25	0.24	0.02	0.26	0.36	0.06	0.09	0.04	0.05
Fe_2O_3	0.10	0.67	0.74	1.50	0.48	0.52	0.19	0.19	0.21	0.23	0.20	0.62	0.21	0.39	1.85	0.13	0.33	0.28	0.21
MgO	30.84	29.2	23.3	19.9	22.4	20.5	21.4	19.1	20.1	18.9	17.8	16.7	14.59	13.40	13.01	11.15	10.63	6.58	8.20
NiO	0.05	6.80	10.32	13.0	13.3	15.4	15.7	15.9	16.60	18.3	18.4	21.0	22.8	23.6	24.8	26.1	28.2	32.7	33.1
MnO	-	0.03	-	0.02	0.02	0.03	0.02	0.01	-	-	0.01	0.12	-	-	-	-	-	-	-
CaO	0.33	0.13	0.29	0.20	0.14	0.14	0.15	0.11	0.05	0.08	0.11	0.16	0.19	0.06	0.27	0.17	0.19	0.24	0.06
Na_2O	-	0.28	0.06	0.58	0.30	0.06	0.14	0.38	0.17	0.22	0.07	0.11	0.07	0.43	0.50	0.08	0.07	0.06	0.05
K_2O	-	0.33	0.09	0.19	0.11	0.14	0.08	0.38	0.13	0.16	0.12	0.16	0.10	0.22	0.36	0.08	0.02	0.04	0.01
H_2O+	8.29	7.91	8.05	7.35	7.57	6.99	7.99	6.91	7.34	7.78	7.44	8.55	7.72	6.66	7.10	8.27	7.57	8.02	8.93
Total	98.29	100.24	100.26	98.32	99.03	99.72	99.87	98.79	100.17	99.16	99.30	99.06	99.30	98.52	99.37	98.41	99.17	98.64	98.79
Si	3.94	3.75	3.97	3.95	3.87	3.94	3.87	3.97	3.93	3.90	3.97	3.87	3.98	3.99	3.87	4.02	3.99	4.03	3.90
Al	0.01	0.02	0.00	0.03	0.03	0.02	0.01	0.03	0.01	0.02	0.02	0.02	0.00	0.01	0.03	-	0.01	-	0.01
Fe III.	0.01	0.03	0.04	0.02	0.03	0.03	0.01	-	0.01	0.01	0.01	0.04	0.01	-	0.10	-	-	-	0.01
Σ Tetr.	3.96	3.80	4.01	4.00	3.93	3.99	3.89	4.00	3.95	3.93	4.00	3.93	3.99	4.00	4.00	4.02	4.00	4.03	3.92
Al	-	-	-	-	-	-	-	-	-	-	-	-	-	0.01	-	0.01	-	0.01	-
Fe III.	-	-	-	0.06	-	-	-	0.01	-	-	-	-	-	0.02	0.01	0.01	0.02	0.02	-
Mg	3.09	2.98	2.40	2.12	2.38	2.16	2.29	2.04	2.12	2.06	1.92	1.87	1.62	1.49	1.47	1.28	1.22	0.78	0.99
Ni	0.01	0.37	0.57	0.75	0.76	0.87	0.91	0.91	0.95	1.08	1.07	1.27	1.36	1.42	1.51	1.62	1.74	2.09	2.16
Σ Oct.	3.10	3.36	2.97	2.93	3.14	3.03	3.20	2.97	3.07	3.14	2.99	3.14	2.98	2.94	2.99	2.92	2.98	2.89	3.15
H_2O+	1.86	1.81	1.86	1.75	1.80	1.65	1.91	1.65	1.74	1.90	1.80	2.15	1.92	1.66	1.79	2.12	1.94	2.13	2.42

Sources of samples.

1. Goles Mountain, Yugoslavia. Supplied by Z. Maksimovic. Additional analyses listed in Brindley et al. (1977).
2. Soroako, Indonesia. Supplied by INCO, #S71-10b
3. Kremze, Bohemia. Supplied by J. Ulrych, described by Slansky (1955).
4. Democrat, N. Carolina. Collected 1974, #74-2
5. Pomalaa, Indonesia. Supplied by INCO, #S71-2c
6. Democrat, N. Carolina. Collected 1974, #74-1b
7. Pomalaa, Indonesia. Supplied by INCO, #S71-1
8. Pomalaa, Indonesia. Supplied by INCO, #S71-43
9. Pomalaa, Indonesia. Supplied by INCO, #S71-1

10. Sua-Sua, Indonesia. Supplied by INCO, #S71-1040.
11. Democrat, North Carolina. Collected 1974, #74-102b
12. Soroako, Indonesia. Supplied by INCO, #S71-1019b
13. Ba, Serbia. Supplied by Z. Maksimovic, #201
14. Soroako, Indonesia. Supplied by INCO, #S71-1003
15. Soroako, Indonesia. Supplied by INCO, #S71-993
16. Frankenstein, L. Silesia. Supplied and described by B. Ostrowicki (1965; Table 8, Sample 4).
17. Ambatondrazaka, Madagascar. Supplied by S. Caillère, M.d'H. N.# 119-228
18. Frankenstein, L. Silesia, Supplied by B. Ostrowicki (1965; Table 8, Sample 6).
19. Bien Venue Mine, Nakety, New Caledonia. Supplied by U.S. Nat. Museum, #108660 (2).

Chemical analyses and formulae

Chemical analyses of nineteen kerolites and pime-lites arranged in order of increasing NiO content are presented in Table 2 together with the sources of the materials. The structural formulae, calculated on the basis of a total cation valence of +22, also are given. Tetrahedral positions are filled with Si ions together with Al and Fe^{3+} ions, if available, to fill four positions. Mg and Ni ions and any remaining Al and Fe^{3+} ions are placed in octahedral positions. The small amounts of Na, K and Ca ions are neglected; they may arise from traces of impurities and/or occupy surface positions. The numbers of ions in tetrahedral and octahedral positions are usually close to 4.0 and 3.0 respectively; in six cases where ΣTetr. falls below 3.95, ΣOcta. rises correspondingly above 3.0 to keep the total valence at +22. If poorly crystalline serpentine minerals are present as impurities, they would tend to raise the ratio of R^{2+} ions to Si^{4+} ions. Taken as a whole, the results confirm that kerolites and pimelites deviate little from a talc-like composition except for the high value of H_2O. The average composition of the nineteen samples in Table 2 is $[(Mg, Ni)_{3.04} (Al, Fe)_{0.01}] (Si_{3.93}Al_{0.02}Fe_{0.02}) O_{10} (OH)_2 \cdot 0.89 \, H_2O$.

Three procedures have been used to study the nature of the additional water: (i) thermogravimetric analyses to ascertain loss of weight (water) as a function of temperature, (ii) dehydration–rehydration experiments to study if water once lost is easily recovered, and (iii) spectroscopic study.

Thermogravimetric curves (typical results are shown in Fig. 7) show a distinct difference between the relatively sharp loss of "hydroxyl" water due to the decomposition of $(OH)_2$, and the gradual loss of the additional water from 110°C to about 730°C. Dehydroxylation occurs between about 730–800°C for kerolites, 730–840°C for nickeloan kerolites, and 800°–900° for pimelites. For fine-grained, well-crystallized talc the corresponding temperature range is 840°–910°C. The long temperature range, 110°–730°C, in which the additional water is lost suggests that it is held by a range of bonding forces. Brindley *et al.* (1977) showed that water lost up to 300°C is almost completely regained and that lost at 650°C is only 70–90 percent regained; the results suggest that much of this water is held by external surfaces as either OH or molecular H_2O.

Spectroscopic study of kerolite and pimelites

Thirteen samples were studied by infrared spectroscopy, and the O–H vibrations in particular were examined in detail. Figure 2 presents near-infrared spectra of a kerolite and a nickeloan kerolite. For all samples this region is dominated by overtones and summations of hydroxyl vibrations in the mid-range infrared. Molecular water is indicated by absorption near 1900 nm, and most of this water is lost by 300°C. The band near 2200 nm is present in all kerolite and pimelite spectra and is possibly an Si–O–H combination band (Scholze, 1960a,b), arising from the Si–O ν_1 and ν_3 modes plus an O–H stretching vibration; a similar band is present in the spectra of finely ground talc and quartz but not in the spectra of the well-crystallized minerals.

Mid-range infrared spectra of kerolites and pime-lites are analogous to that of talc, with broadened absorptions and additional adsorptions due to hydroxyl and adsorbed water. Figure 3 shows typical spectra of several nickeloan kerolites, pimelites, and a nickeloan talc, $Ni_{1.74}Mg_{1.22}Si_4O_{10}(OH)_2$, in the range of 300–4000 cm^{-1}. Figures 4 and 5 show more detailed spectra in the range 3000–4000 cm^{-1} and 600–800 cm^{-1} respectively. Absorptions of particular interest are those at 670–700 cm^{-1} assigned to a librational motion of structural hydroxyl, the water bending vibration near 1600 cm^{-1}, and various hydroxyl stretching vibrations between 3400 and 3700 cm^{-1}. The broad band at about 3400 cm^{-1} is due to adsorbed water, and the various sharper bands between 3630 and 3680 cm^{-1} are due to structural hydroxyl. The spectra in Figure 4 show the 3600 and 3700 cm^{-1} absorptions to varying degrees; as Brindley *et al.* (1977) noted, the adsorption at 3600 cm^{-1} is attributed to O–H stretching associated with H-bonds between interlayer water and surface oxygens, and the absorption at about 3700 cm^{-1} is attributed to vibrations of surface OH groups. Virtually all spectra show this high-frequency OH vibration, although to varying degrees.

The behavior of the nickeloan kerolites and pime-lites with increasing temperature is the same as that of kerolites; the amount of adsorbed water decreases reversibly, and the absorption at about 3700 cm^{-1} decreases irreversibly after heating to 600°C. Accompanying the large reduction in the intensity of the 3700 cm^{-1} absorption is a decrease in the shoulder between 850 and 900 cm^{-1} adjacent to the 1014 cm^{-1} Si–O vibration. This shoulder may be due to Si–O stretching of Si–OH groups; such groups are characterized by similar shifts in the Si–O absorption band of silica gels (Moenke, 1974, p. 369).

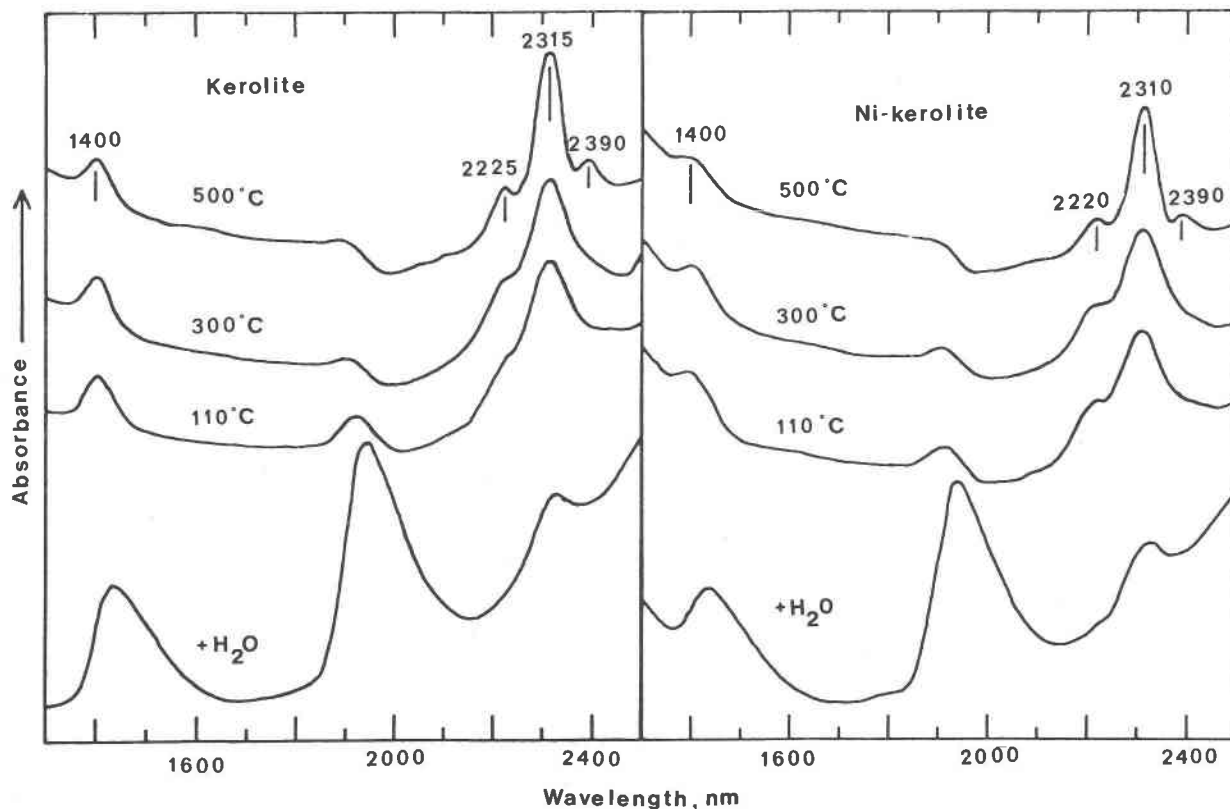Infrared spectroscopy also provides evidence of changes taking place with increasing nickel sub-

Fig. 2. Near-infrared spectra of kerolite (Carter's Mine, N. Carolina; chem. anal. in Brindley *et al.,* 1977, p. 448; sample 481.90) and nickeloan kerolite (Sample 6, Table 2).

stitution. Hydroxyl stretching in pure well-crystallized talc occurs at about 3680 cm^{-1}, and kerolites containing little or no nickel exhibit a broad absorption close to 3680 cm^{-1} which sharpens appreciably after heating to 660°C. As noted by several investigators (Vedder, 1964; Wilkins and Ito, 1967; DeWaal, 1970), with an increase in nickel content, up to four O–H stretching absorptions are possible. These correspond to the four possible combinations of the nickel and magnesium ions in the three octahedral sites linked to a hydroxyl, *i.e.,* (Mg,Mg,Mg), (Mg,Mg,Ni), (Mg,Ni,Ni), and (Ni,Ni,Ni) (Wilkins and Ito, 1967). The absorption in the 3680 cm^{-1} region of the kerolite spectra does indeed split with increasing nickel, but four individual absorptions are not observed. The spectrum in the region 3000–4000 cm^{-1} of the nickeloan talc mentioned previously is compared in Figure 4 with those of a series of kerolites and pimelites with increasing nickel contents. As the amount of nickel increases, additional absorptions become noticeable at about 3645 cm^{-1} and 3625

cm^{-1}, corresponding to the arrangements (Mg,Ni,Ni) and (Ni,Ni,Ni) respectively, and are very close to corresponding absorptions in the nickeloan talc. It is strange that an absorption corresponding to the arrangement (Mg,Mg,Ni) does not appear. The intensities of the 3680 and 3625 cm^{-1} absorptions are approximately equal when the composition is between Mg$_2$Ni$_1$ and Mg$_{1.5}$Ni$_{1.5}$, and the 3625 cm^{-1} absorption becomes stronger with more nickel. Inspection of Figure 4 reveals that there is no rigorously systematic variation in hydroxyl stretching band intensities with composition for the kerolites and pimelites; the majority of the spectra have 3625 cm^{-1} bands with intensities higher than the calculated value. Thus, it appears that the hydroxyl stretching vibrations in kerolites and pimelites are not particularly useful for composition or ordering determinations, as they are for well-crystallized talcs (see Vedder, 1964).

The relative intensities of the absorptions at 670 and 705 cm^{-1} also have been used to estimate compo-

sitions (Stubican and Roy, 1961). Equal intensities of the two bands indicates a Ni:Mg ratio of about 2:1. Figure 5, displaying the region between 600 and 800 cm^{-1}, shows the effects of Ni-for-Mg substitution and reveals a gradual increase in the 705 cm^{-1} band with increasing nickel; for qualitative analysis of the Ni:Mg ratio in these minerals, this region appears suitable.

The effects and nature of the Ni-for-Mg substitution also can be examined by optical absorption spectroscopy which enables us to describe quantitatively the color of the minerals and the coordination and oxidation state of the nickel. Typical spectra are shown in Figure 6 and the individual absorptions are listed and assigned in Table 3. All spectra are consistent with the presence of octahedrally-coordinated Ni^{2+} ions and agree with spectra of other Ni^{2+}-containing minerals in the literature (White *et al.*, 1971; Faye, 1974; Wood, 1974). Bands at about 380, 660, and 1130 nm are spin-allowed transitions, and shoulders at about 425 and 715 nm are assigned to spin-forbidden transitions using the energy-level diagram calculated by Berkes (1968). The band at about 1400 nm is due to an OH overtone vibration and is not electronic in nature. The green color of these minerals is due to the "window" at about 530 nm between the 380 and 660 nm absorptions.

The crystal field splitting parameter, Dq, which is a measure of the strength of interaction between the Ni^{2+} ion and its surroundings, is given by Dq = 1/10ν_1. Dq is directly related to the crystal field stabilization energy by a factor 6/5. The Racah B parameter, obtained by analytically solving the Tanabe–Sugano matrices, is

$$B = \frac{(\nu_3 - 2\nu_1)(\nu_3 - \nu_1)}{3(5\nu_3 - 9\nu_1)}$$

and is related to the "covalency" of the Ni–O bond. The Dq and B parameters are included in Table 3. Values of Dq, which range from about 850 to 900 cm^{-1} and average 885 cm^{-1}, are close to the values for nickeloan chrysotile, 910 cm^{-1} (Faye, 1974), MgO:Ni^{2+}, 860 cm^{-1}, and CaNiSi$_2$O$_6$, 840 cm^{-1} (White *et al.*, 1971). The plot of Dq *vs.* M–O bond distance constructed by Faye (1974) gives an average Ni–O bond length of 2.06±0.02A, in good agreement with the average Mg–O bond distance in talc of 2.07A (Rayner and Brown, 1973). The Racah B parameter averages 950 cm^{-1}, compared with 947 cm^{-1} for nickeloan chrysotile (Faye, 1974) and 1030, 858, 881, and 1039 cm^{-1} for the free Ni^{2+} ion, MgO:Ni^{2+},
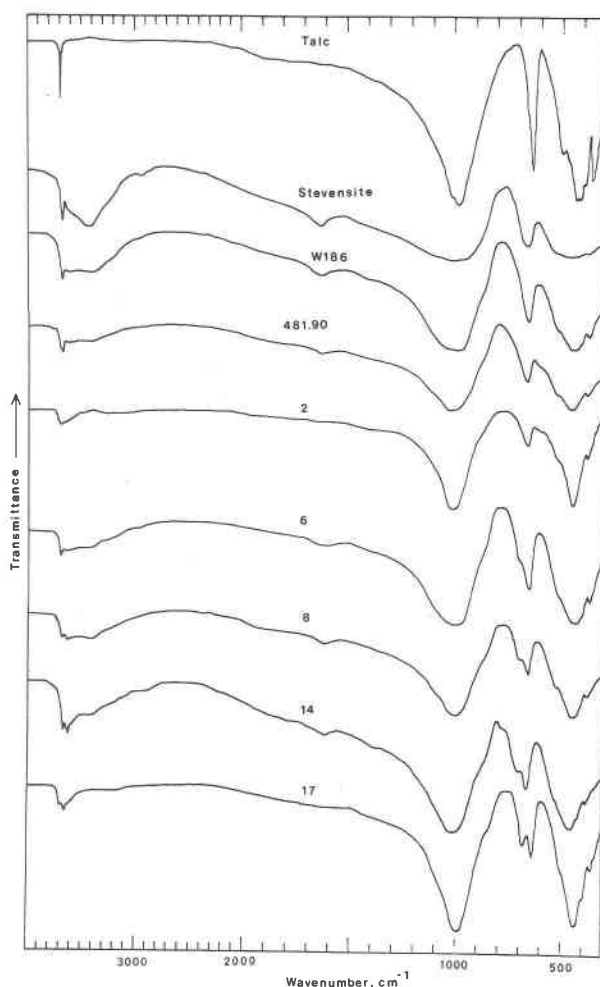

Fig. 3. Infrared spectra of talc (fine-grained, Manchuria), stevensite (NMNH, R4710; Faust and Murata, 1953), kerolites (W 186 and 481.90; Brindley *et al.*, 1977, p. 448). All other samples, see Table 2.

CaNiSi$_2$O$_6$, and nickeloan clinoenstatite respectively (White *et al.*, 1971). We find no evidence for the existence in the natural unheated minerals of trivalent nickel or for Ni^{2+} in other than octahedral coordination.

Thermal transformations

The phases formed by heating kerolites, nickeloan kerolites, and pimelites to temperatures of about 1000°C were discussed by Pham Thi Hang and Brindley (1973). They observed that kerolites gave enstatite as the main product, and that nickel-containing forms gave first an enstatite product with little olivine, but subsequently olivine with minor enstatite.
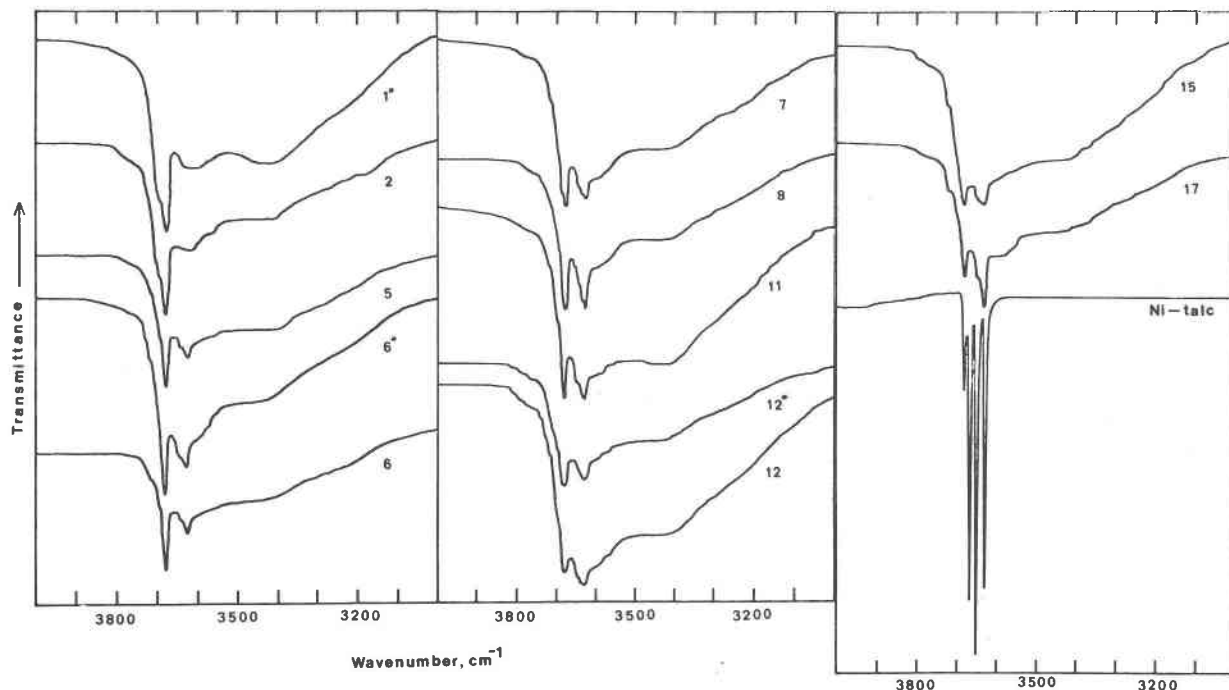
Fig. 4. Hydroxyl-stretching region of the infrared spectra of kerolites, pimelites and nickeloan talc. Simple descriptions given mainly in Table 2. Additionally, sample 1* is a kerolite, W186, described by Brindley *et al.* (1977, p. 448); samples 6* and 12* are from the same veins as samples 6 and 12 respectively and illustrate variations within one vein.
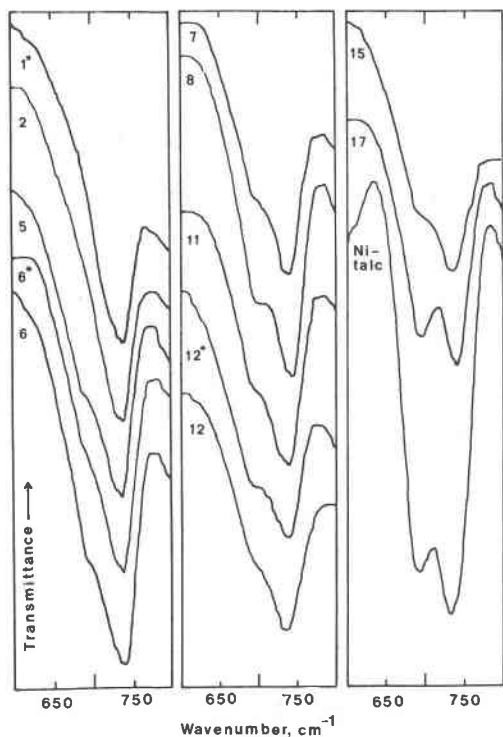

Fig. 5. Hydroxyl-libration region of the infrared spectra of kerolites, pimelites, and nickeloan talc. For sample designations, see Fig. 4.

The influence of the initial structure as distinct from the total composition was uncertain because the initial samples appeared to have considerable proportions of a serpentine component.

We have examined the phases formed by heating small samples in platinum thimbles for periods of 3–4 hr at temperatures of 710, 855, 960, 1080 and 1230°C. Figure 7 shows schematically the results obtained for four samples: (i) kerolite from Wiry Mine, L. Silesia, given by Antoni Wala, Cracow, Poland, which is quite similar to sample (1) in Table 2; (ii) nickeloan kerolite, sample (3) of Table 2; (iii) and (iv) pimelites, samples (17) and (18) of Table 2. Each section of Figure 7 shows the thermogravimetric weight-loss curve and the amounts of hydroxyl water, marked 2(OH), and additional water. The stippled areas show the variation of the basal reflected intensities as the minerals are heated; evidently little change in the original structure occurs until dehydroxylation begins around 700–800°C. Enstatite, marked E, is the first product phase in all cases, together with a poorly defined phase marked FCC which may be face-centered cubic (see later). In agreement with the earlier work, enstatite remains as the final phase formed by kerolites, but pimelites develop an olivine-type phase near 1000°C, marked F in Figure 7. Nickeloan kero-
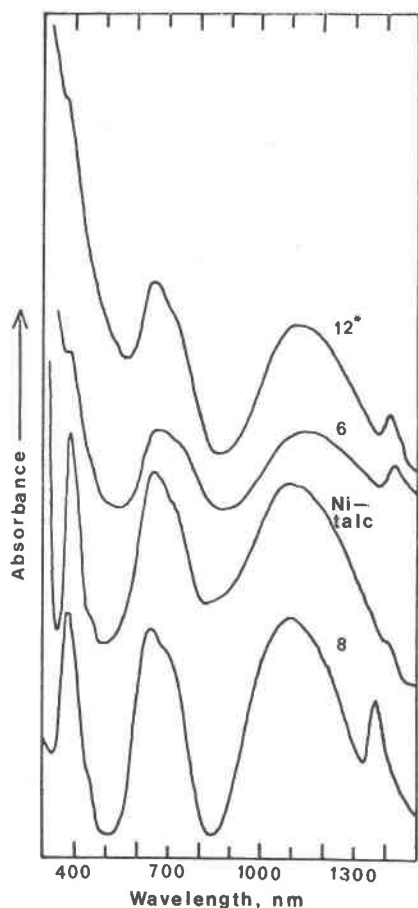
Fig. 6. Visible absorption spectra of nickeloan kerolites and nickeloan talc. For sample designations, see Fig. 4.

lites retain both the enstatite (E) and forsterite (F) phases at 1200°C. Cristobalite (marked Cr) also is observed.

These results agree broadly with the equilibrium diagram of the MgO–NiO–SiO₂ system at 1400°C given by Campbell and Roeder (1968). Our present work, however, is concerned more particularly with the sucession of phases when the minerals are heated than with the ultimate equilibrium. Two results are noteworthy. In the first place, enstatite develops first from the talc-like initial structures irrespective of the relative proportions of Mg and Ni. This result reflects the fact that talc transforms topotactically to enstatite when dehydroxylation occurs (Nakahira, 1964). The lattice parameters of the enstatite are related very simply to those of talc, so that this transformation presumably takes place easily. The forsterite phase requires considerably more structural reorganization; it does not develop from low-nickel kerolites but is

obtained from high-nickel kerolites and pimelites. The appearance of this phase in nickel-containing samples is due presumably to the instability of the nickel analog of enstatite.

A second interesting feature is the transitional development of the FCC phase. Figure 8 reproduces diffractometer patterns of pimelite sample 18 of Table 2 after various heat treatments. The broad FCC reflections, respectively (111), (200) and (220), are sketched by the dashed line. In the earlier study of the lizardite–nepouite series, no enstatite phase was recorded and an FCC phase was seen immediately prior to the formation of olivine. The FCC phase is less obvious in the present study, but there is little doubt of its formation. The broad reflections indicate very small crystals. In the temperature range 800°–1000°C, the initial green color of the minerals changes to black, and the higher the nickel content, the deeper is the black color. Beyond 1100°C, the green color is restored due to Ni²⁺ in the olivine. The black color and the FCC phase could well be due to the formation of a defective NiO. The estimated lattice parameter, 4.2–4.3A, can be compared with 4.178A for NiO and 4.213 for MgO; mixed oxides, (Mg,Ni)O, have intermediate parameters.

Acknowledgments

Table 3. Visible absorptions and assignments for nickeloan kerolites and nickeloan talc

Samples[a]	6	8	10	Ni-talc	Assignment
ν_1 (nm) [b]	1131	1117	1138	1113	$^3A_{2g}(F) \rightarrow {}^3T_{2g}(F)$
"		725	703	717	714	$^1E_{(D)}$
ν_2 (nm)	660	648	658	654	$^3T_{1g}(F)$
"		442	445	–	451	$^1T_{2g}(D), {}^1A_{1g}(G)$
ν_3 (nm)	385	383	370	392	$^3T_{1g}(P)$
Dq (cm^{-1})	884	895	878	898	
B (cm^{-1})	941	939	1025	890	
% NiO	15.4	15.9	18.4	28.2	

(a) Sample numbers 6, 8 and 10 refer to those in Table 3.

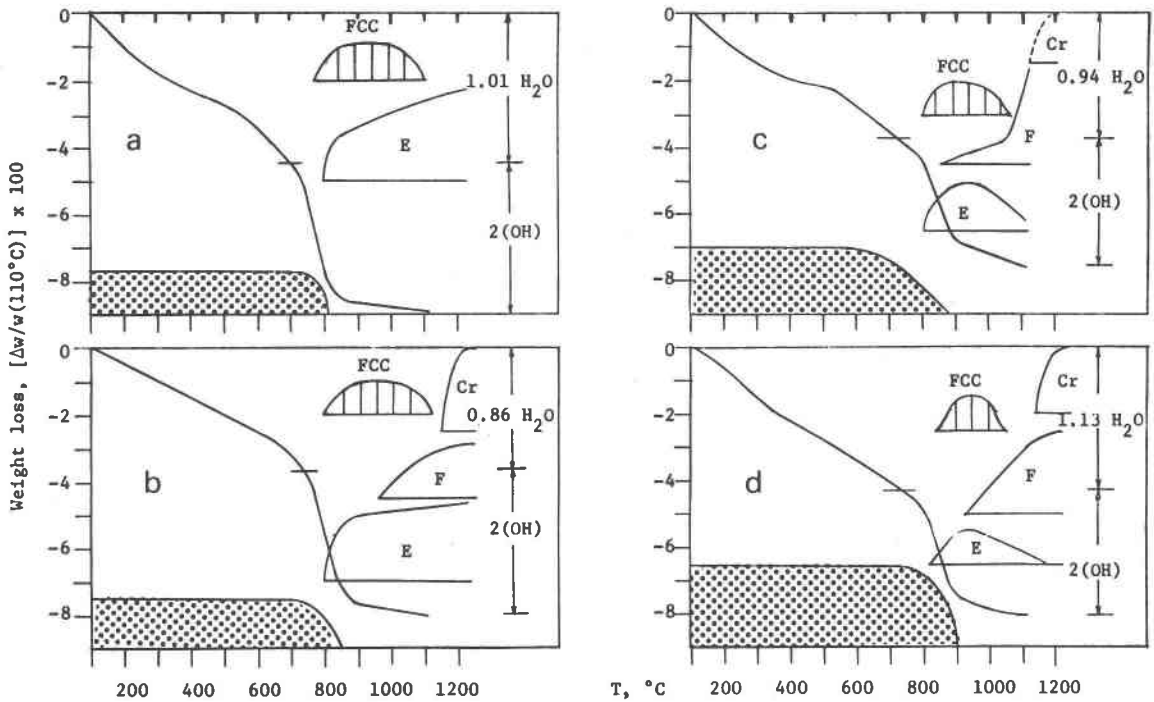(b) Wavelengths are accurate to ± 10 nm.

Fig. 7. Thermal transformation data for (a) kerolite, W186, see caption to Fig. 4; (b) nickeloan kerolite, sample (3), Table 2; (c) and (d) pimelites, samples (17), (18), Table 2. Stippled areas indicate persistence of initial minerals. Phases formed: E = enstatite, F = olivine-type phase, Cr = cristobalite, FCC = face-centered cubic phase. Each diagram shows thermogravimetric weight-loss curve. Arrows indicate hydroxyl water loss and molecular water loss.
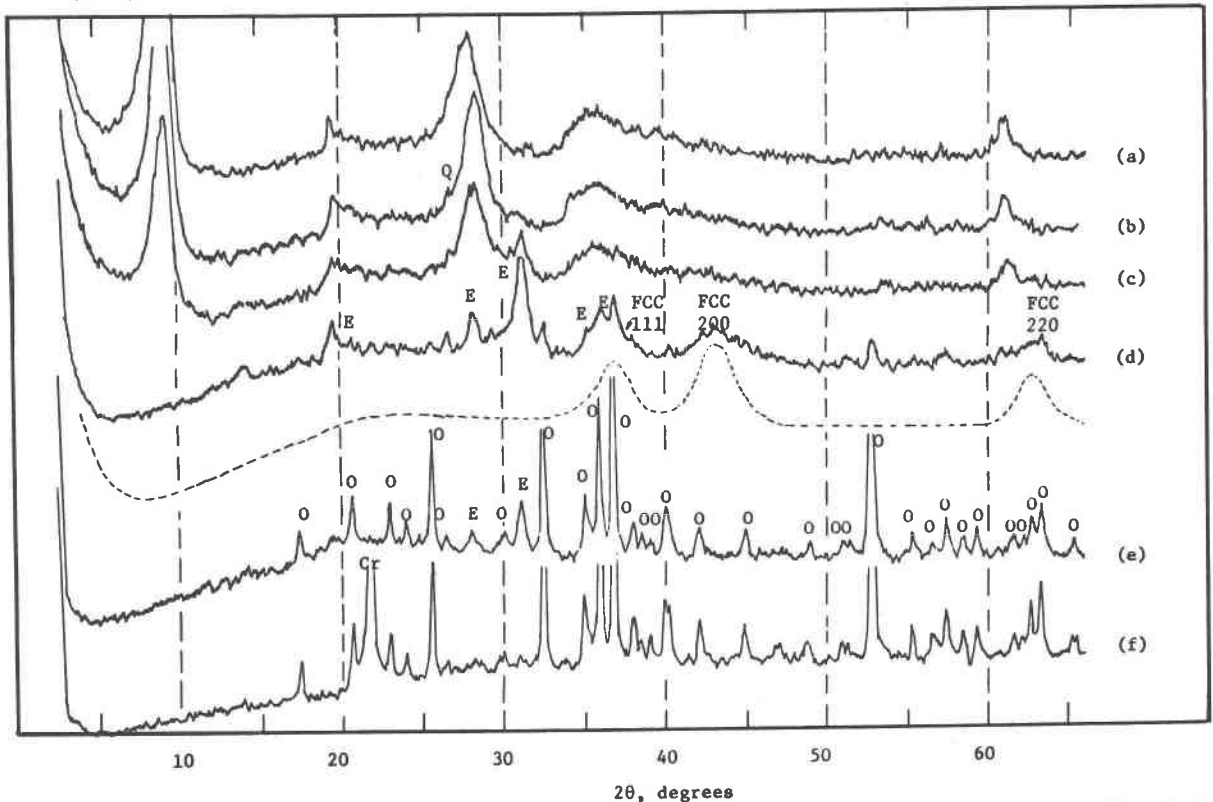

Fig. 8. Diffractometer patterns of pimelite, sample (18) of Table 2, CuKα radiation. (a) Room temperature; (b)–(f) after 4 hrs heat treatment at 710°, 855°, 960°, 1080°, 1230°C. Diffraction peaks labelled as follows: Q = quartz, E = enstatite, O = olivine-type phase, FCC = face-centered cubic phase.

References

Berkes, J. S. (1968) *Energy level diagrams for transition metal ions in cubic crystal fields.* MRL Monograph No. 2. Materials Research Laboratory, The Pennsylvania State University.

Bish, D. L. and G. W. Brindley (1978) Deweylites, mixtures of poorly crystalline hydrous serpentine and talc-like minerals. *Mineral. Mag., 42,* 75–80.

Brindley, G. W., David L. Bish and H.-M. Wan (1977) The nature of kerolite, its relation to talc and stevensite. *Mineral. Mag., 41,* 443–452.

—— and G. Ertem (1971) Preparation and solvation properties of some variable charge montmorillonites. *Clays Clay Minerals, 19,* 399–404.

—— and Z. Maksimovic (1974) The nature and nomenclature of hydrous nickel-containing silicates. *Clay Minerals, 10,* 271–277.

—— and Pham Thi Hang (1973) The nature of garnierites—I. Structures, chemical compositions, and color characteristics. *Clays Clay Minerals, 21,* 27–40.

—— and H.-M. Wan (1975) Compositions, structures and thermal behavior of nickel-containing minerals in the lizardite–nepouite series. *Am. Mineral., 60,* 863–871.

Campbell, F. E. and P. Roeder (1968) The stability of olivine and pyroxene in the Ni–Mg–Si–O system. *Am. Mineral., 53,* 257–268.

DeWaal, S. A. (1970) Nickel minerals from Barberton, South Africa: III. Willemseite, a nickel-rich talc. *Am. Mineral., 55,* 31–42.

Faye, G. H. (1974) Optical absorption spectrum of Ni^{2+} in garnierite: a discussion. *Can. Mineral., 12,* 389–393.

Giese, R. F. (1975) Interlayer bonding in talc and pyrophyllite. *Clays Clay Minerals, 23,* 165–166.

Maksimovic, Z. (1966) β-Kerolite–pimelite series from Goles Mountain, Yugoslavia. *Proc. Int. Clay Conf., Jerusalem 1,* 97–105.

Medlin, J. H., N. H. Suhr, and J. B. Bodkin (1964) Atomic absorption analysis of silicates employing $LiBO_2$ fusion. *Atomic Absorption Newsletter, 8,* 25–29.

Moenke, H. H. W. (1974) Silica, the three-dimensional silicates, borosilicates and beryllium silicates. In V. C. Farmer, Ed., *The Infrared Spectra of Minerals,* p. 365–382. Mineralogical Society, London.

Nakahira, M. (1964) Thermal transformations of pyrophyllite and talc as revealed by X-ray and electron diffraction studies. *Clays Clay Minerals, 12,* 21–27.

Ostrowicki, B. (1965) Mineraly niklu strefy wietrzenia serpentynitow w Szklarach [Nickel minerals of the weathering zone of serpentinites at Szklary (Lower Silesia)]. *Polska Akad. Nauk, Prace Mineral., 1,* 7–87 (with English summary, 88–92).

Pecora, W. T., S. W. Hobbs, and K. J. Murata (1949) Variations in garnierite from the nickel deposit near Riddle, Oregon. *Econ. Geol., 44,* 13–23.

Pham Thi Hang and G. W. Brindley (1973) The nature of garnierites—III. Thermal transformations. *Clays Clay Minerals, 21,* 51–57.

Rayner, J. H. and G. Brown (1973) The crystal structure of talc. *Clays Clay Minerals, 21,* 103–114.

Scholze, H. (1960a) Zur Frage der Unterscheidung zwischen H_2O Molekulen und OH-Gruppen in Gläsern und Mineralen. *Naturwissenschaften, 47,* 226–227.

—— (1960b) Eine weitere Unterscheidungsmöglichkeit ob in Gläsern H_2O-Moleküle oder OH-Gruppen vorliegen. *Glastech. Ber., 33,* 33.

Slansky, E. (1955) The Ni-hydrosilicates from Kremze in South Bohemia. (Czech text, English abstract). *Univ. Carol., Geol. 1,* 1–28.

Stubican, V. and R. Roy (1961) A new approach to assignment of infrared absorption in layer-structure silicates. *Z. Kristallogr., 115,* 200–214.

Vedder, W. (1964) Correlations between infrared spectrum and chemical composition of mica. *Am. Mineral., 49,* 736–768.

Warren, B. E. and P. Bodenstein (1965) The diffraction pattern of fine particle carbon blacks. *Acta Crystallogr. 18,* 282–286.

White, W. B., G. J. McCarthy, and B. E. Scheetz (1971) Optical spectra of chromium, nickel, and cobalt-containing pyroxenes. *Am. Mineral., 56,* 72–89.

Wilkins, R. W. T. and J. Ito (1967) Infrared spectra of some synthetic talcs. *Am. Mineral., 52,* 1649–1661.

Wood, B. J. (1974) Crystal field spectrum of Ni^{2+} in olivine. *Am. Mineral., 59,* 244–248.